Manuscript Information

Journal name: Nature methods
NIHMS ID: NIHMS1520040
Manuscript Title: Aromatic 19F-13C TROSY: A background-free probe of biomolecular structure, function and dynamics
Submitter: Nature Publishing Group (repositorynotifs@nature.com)

Manuscript Files

Type	Fig/Table #	Filename	Size	Uploaded
manuscript	1	article_1.docx	152787	2019-01-31 03:37:51
figure	1	figure_1.eps	968546	2019-01-31 03:37:51
figure	2	figure_2.eps	1177902	2019-01-31 03:37:51
figure	3	figure_3.eps	1488214	2019-01-31 03:37:51
figure	4	figure_4.eps	2608042	2019-01-31 03:37:51
figure	5	figure_5.eps	3449226	2019-01-31 03:37:51
figure	6	figure_6.eps	983834	2019-01-31 03:37:51
supplement	Reporting Summary	supp_info_2.pdf	67762	2019-01-31 03:37:51
supplement	Supplemental Information	supp_info_1.pdf	243392	2019-01-31 03:37:51
supplement	Supplementary Figures	43634_3_supp_469173_pjjn82.docx	5928629	2019-04-29 11:18:26
supplement	Supplementary	43634_3_data_0_pm5lkm.zip	345165	2019-04-29

	Software			11:18:22

Aromatic ^{19}F-^{13}C TROSY: A background-free approach to probe biomolecular structure, function and dynamics

Andras Boeszoermenyi[1,2]†, Sandeep Chhabra[1,2,8]†, Abhinav Dubey[1,2], Denitsa L. Radeva[3], Nikola T. Burdzhiev[3], Christo D. Chanev[3], Ognyan I. Petrov[3], Vladimir M. Gelev[3], Meng Zhang[1], Clemens Anklin[4], Helena Kovacs[5], Gerhard Wagner[1], Ilya Kuprov[6], Koh Takeuchi[7*], Haribabu Arthanari[1,2*]

1 Department of Biological Chemistry and Molecular Pharmacology, Harvard Medical School, Boston, USA

2 Department of Cancer Biology, Dana-Farber Cancer Institute, Boston, MA, USA

3 Faculty of Chemistry and Pharmacy, Sofia University, 1 James Bourchier, Sofia 1164, Bulgaria

4 Bruker Biospin Billerica, MA, USA

5 Bruker Biospin, Fällanden, Switzerland

6 School of Chemistry, University of Southampton, Highfield, Southampton SO17 1BJ, UK

7 Molecular Profiling Research Center for Drug Discovery (Molprof), National Institute of Advanced Industrial Science and Technology (AIST), Tokyo 135-0064, Japan

8 Medicinal Chemistry, Monash Institute of Pharmaceutical Sciences, Monash University, Parkville, Victoria, 3052, Australia

† These authors contributed equally to this work.

*Correspondence to:

E-mail: hari@hms.harvard.edu or koh-takeuchi@aist.go.jp

Abstract: Obtaining atomic level information about the structure and dynamics of biomolecules is critical to understand their function. Nuclear magnetic resonance (NMR) spectroscopy provides unique insights into the dynamic nature of biomolecules and their interactions, capturing transient conformers and their features. However, relaxation-induced line broadening and signal overlap make it challenging to apply NMR to large biological systems. Here, we take advantage of the high sensitivity and the broad chemical-shift range of ^{19}F nuclei, and leverage the remarkable relaxation properties of the aromatic ^{19}F-^{13}C spin pair to disperse ^{19}F resonances in a 2-dimensional transverse relaxation optimized TROSY spectrum. We demonstrate the application of the ^{19}F-^{13}C TROSY to investigate proteins and nucleic acids. This experiment expands the scope of ^{19}F NMR in the study of structure, dynamics and function of large and complex biological systems and provides a powerful background-free NMR probe.

Introduction: Obtaining structural and dynamics information on biomolecules is critical for understanding their functions and mechanisms. Solution-state nuclear magnetic resonance (NMR) spectroscopy provides such information at atomic resolution and in a quantitative manner. A main advantage of NMR is that it queries individual atoms within a biomolecule to provide information on structure and local and global dynamics. However, extracting such information relies heavily on the ability to resolve individual atomic resonances. Spectral complexity and line broadening severely limit the application of NMR, particularly for larger systems.

One of the most impactful developments in biomolecular NMR has been the implementation of transverse relaxation optimized spectroscopy (TROSY)[1, 2]. The transverse relaxation rate (R_2) determines the width of the NMR signal and it increases with the size of the

system. Therefore, signals originating from larger biomolecules are broader. Two major factors that determine R_2 at high magnetic field strengths are chemical shift anisotropy (CSA) and the dipole-dipole relaxation (DD). The TROSY experiment selects a component of the NMR signal for which CSA and DD negate each other, resulting in narrower lines. TROSY has enabled studies of large systems such as the 670 kDa 20S proteasome[3] and the 900 kDa GroEL-GroES complex[4].

Despite these advances, NMR studies of biomolecules larger than 30 kDa remain far from routine and need further methodological developments. Fluorine-19 (^{19}F) NMR is re-emerging as a preferred method to detect weak interactions in biomolecules and to study the structure and dynamics of proteins and nucleic acids. ^{19}F NMR provided early evidence of scalar coupling[5] and the nuclear Overhauser effect[6] in the 1950s and was introduced into biological NMR in the 1970s[7]. However, its use for study of biological systems has been limited due to the rapid ^{19}F-CSA-driven relaxation that occurs at high magnetic fields. Nevertheless, the power of ^{19}F NMR has been illustrated by studying GPCR dynamics using site-specific-CF_3 labelling strategies[8, 9]. ^{19}F NMR has also been used to probe DNA duplex formation[10], site-specific RNA binding[11], RNA invasion[12], and telomeric RNA G-quadruplex structures in vitro and in living *cells*[13].

^{19}F is one of the most NMR sensitive nuclei due to its large gyromagnetic ratio (γ = 0.941 relative to ^{1}H), 100% natural abundance, and a large chemical shift range of ~200 ppm in biological systems[14]. Uniquely, ^{19}F is not naturally present in biomolecules, rendering ^{19}F NMR background-free and thus especially useful for *in cell* NMR experiments[15, 16]. The main disadvantage of ^{19}F is its large CSA, which broadens ^{19}F resonances in high molecular weight systems, even at relatively low magnetic field strengths.

To address this problem and enhance the utility of ^{19}F NMR spectroscopy, we developed a 2-dimensional (2D) ^{19}F-^{13}C TROSY experiment. Our theoretical calculations show that the ^{19}F-^{13}C TROSY effect is applicable for ten different ^{19}F incorporations in aromatic amino acids and eight ^{19}F substitutions in nucleobases. Intriguingly, the mutual cancellation of the CSA and DD in aromatic ^{19}F-^{13}C systems yields TROSY resonances for ^{13}C nuclei bonded to ^{19}F ($^{13}C_F$) that are significantly narrower than those of the corresponding ^{13}C resonances bonded to ^{1}H ($^{13}C_H$). We use a ^{13}C-detected experiment with TROSY selection to directly observe these narrow $^{13}C_F$ resonances, which results in excellent spectral resolution. We provide both the theoretical and experimental framework for ^{19}F-^{13}C TROSY experiments and validate the approach on the 7 kDa protein G B1 domain (GB1)[17], the 42 kDa maltose binding protein (MBP)[18], and the 180-kDa α7 single-ring of the 20S proteasome core particle (CP) from *Thermoplasma acidophilum*[3, 19], as well as a 16-mer, double-stranded DNA at low temperature.

Results:

^{19}F-^{13}C DD-CSA cross-correlation in 3-$^{19}F^{13}C$ Tyr and the TROSY effect

While R_2 in spin ½ nuclei like ^{19}F and ^{13}C is dominated by DD and CSA mechanisms, their individual contribution can vary. In the case of aromatic ^{19}F-^{13}C systems, the line width is dominated by the CSA mechanism, especially at high magnetic fields. We calculated chemical shielding tensors for ten ^{19}F-^{13}C spin pairs at various positions in aromatic amino acid side chains using DFT methods (Supplementary Note I; axiality and rhombicity parameters of the CSA tensors are collected in Supplementary Table 1) and then used the Bloch-Redfield-Wangsness relaxation theory module available in the *Spinach*[20] library to compute the R_2

relaxation rates for each ^{13}C-^{19}F pair (Supplementary Fig. 1). While there are variations in R_2, dependent on the amino acid type and ^{19}F position, the calculations indicate that the R_2 of the TROSY component of $^{13}C_F$ is 3 to 18-fold slower than that of the corresponding decoupled resonance. Thus, selective detection of the $^{13}C_F$ TROSY resonance would yield sensitive, high-resolution NMR spectra for ^{19}F-^{13}C pairs in any aromatic amino acid.

CSA contribution to the R_2 scales quadratically with the magnetic field, while the DD contribution is much less sensitive to increase in magnetic field strength. This is reflected in the magnetic-field-dependent increase in R_2 calculated for decoupled resonances (e.g.: 3-^{19}F Tyr; Fig.1, blue triangles). However, CSA relaxation that is comparable to DD relaxation often generates favourable DD-CSA cross-correlation, which makes one of the components of the $^{13}C_F$ coupled doublet relax slower compared to the other (Fig. 1a, red squares). Which doublet component relaxes slower depends on the angles between the DD and the CSA tensor axes, and on the sign of the *J*-coupling. The narrower (slower relaxing) line is referred to as the transverse-relaxation-optimized "TROSY" line[1, 2]. For the $^{13}C_F$ resonances, our estimates indicate that the TROSY component of the $^{13}C_F$ doublet relaxes 8.7 times slower (6.1 s^{-1}) compared to the decoupled signal (53 s^{-1}) for 3-^{19}F Tyr incorporated in a 42 kDa protein at 600 MHz (^1H frequency; τ_c = 25 ns at 25 °C) (Fig. 1a). By comparison, the TROSY components of $^{13}C_H$ resonances relax with a rate of 43 s^{-1} (Fig. 1b) under identical conditions. On the other hand, the TROSY effect on the $^{19}F_C$ and ^1H_C resonances is rather small (Fig. 1c and Fig. 1d). Thus, selective detection of TROSY resonances from $^{13}C_F$ would allow detection of the ^{19}F-^{13}C pair with high sensitivity and resolution.

Experimental observation of ^{19}F-^{13}C TROSY effect from 1D ^{13}C spectra

In order to harness the power of aromatic ^{19}F-^{13}C TROSY selection and to avoid splitting of ^{13}C resonances by the one-bond C-C coupling ($^{1}J_{CC}$ ~60Hz), we synthesized a selectively ^{13}C-labeled and fluorinated tyrosine, 3,5-$^{13}C_2$-3-fluoro-L-tyrosine, which has a ^{19}F-^{13}C pair at the 3rd position in the aromatic ring (3-$^{19}F_{13C}$ Tyr), using a modified method described by Kitevski-LeBlanc *et al.*[21]. To demonstrate the applicability of the ^{19}F-^{13}C TROSY experiment, we expressed two model systems, a small protein, G B1 domain (GB1), and a larger protein system, maltose binding protein (MBP) in *E. coli* using 3-$^{19}F_{13C}$ Tyr.

GB1 (τ_c = 5 ns) which harbours three tyrosine residues, gives three resonance pairs in its 1D ^{13}C spectrum, each of which are separated by ~240 Hz, the expected ^{19}F -^{13}C ($^{1}J_{CF}$) coupling value (Fig. 2a). The TROSY effect is clearly seen in these 1D spectra acquired at different field strengths. The TROSY resonances which are up-field are intense and narrow while the down-field anti-TROSY signals are weak and broad. ^{1}H decoupling was applied during acquisition to remove remote (>two-bond) ^{1}H couplings. Although our labelling technique removed the strong one-bond ^{13}C-^{13}C coupling ($^{1}J_{CC}$ ~ 60Hz), the ^{13}C-labeling at the 5th position in the aromatic ring, originating from the stable-isotope precursor, caused a two-bond ^{13}C-^{13}C coupling ($^{2}J_{CC}$ ~7 Hz). The narrow TROSY lines make this small coupling clearly visible in the 1D ^{13}C spectra as a testament to the resolution gain (Fig. 2a).

To compare the effect of TROSY on $^{13}C_F$ and $^{13}C_H$ resonances at equivalent positions, we recorded a 1D ^{13}C spectrum of unlabelled GB1 using natural abundance ^{13}C, to negate the $^{1}J_{CC}$ coupling. Although the TROSY effect can be seen clearly in the sharper, more intense up-field TROSY component of the $^{13}C_H$ resonances, the linewidths are much broader than those of $^{13}C_F$ (Fig. 2b), highlighting the effect of the significantly slower R_2 of $^{13}C_F$. It should be noted that to see the TROSY effect, ^{1}H decoupling could not be applied during $^{13}C_H$ detection and therefore

the remote ^{1}H couplings contribute to the line broadening. Nevertheless, unlike the very narrow $^{13}C_F$ lines, which allowed resolution of the 7Hz $^{2}J_{CC}$ couplings, the broader lines of the $^{13}C_H$ nuclei obscure the individual detection of these remote couplings. Of note, TROSY resonance of $^{13}C_F$ is the up-field component, whereas the TROSY resonance of $^{13}C_H$ is the down-field component due to the opposite sign of the ^{19}F-^{13}C and ^{1}H-^{13}C ^{1}J-coupling (negative and positive, respectively).

The 2D ^{19}F-^{13}C TROSY experiment

Our 1D-$^{13}C_F$ data indicated the need to choose the up-field $^{13}C_F$ component for TROSY selection in a 2D ^{13}C-^{19}F TROSY experiment. Theoretical calculations showed that the $^{19}F_C$ TROSY component relaxed more slowly as compared to the decoupled resonance. To observe the TROSY effect on $^{19}F_C$ and choose the correct TROSY resonance we recorded decoupled and coupled ^{13}C-^{19}F HSQCs of MBP (Supplementary Fig. 2). The coupled spectrum showed that the up-field ^{19}F component was narrower, which, when taken together with the 1D-^{13}C results, indicates that the top-right resonance is the TROSY component.

To selectively choose the TROSY resonance we designed an experiment with an ST2PT pulse scheme for TROSY selection (^{13}C-^{19}F TROSY-SE), similar to that used for the ^{15}N-^{1}H TROSY-HSQC[22] (Supplementary Fig. 2). In this sensitivity enhanced pulse-sequence design, the experiment starts with and ends on ^{19}F magnetization, the nucleus with the larger gyromagnetic ratio, with the ^{13}C frequency encoded in the indirect dimension. However, while the experiment worked well for GB1, the experiment was not sufficiently sensitive for the higher molecular

weight protein MBP (42 kDa), as we were not able to observe all the fifteen 3-$^{19}F_{13C}$ Tyr resonances at 25 °C. We hypothesized that this was due to faster relaxation of the $^{19}F_C$ nuclei. The CSA of $^{19}F_C$ accelerates its relaxation significantly and is the primary reason for the poor sensitivity observed in the ^{13}C-^{19}F TROSY-SE experiment. Indeed, shortening the experiment by removing the sensitivity enhancement block had no significant effect on signal intensity, as the reduction in time cancels the gain of the sensitivity enhancement block (Supplementary Fig. 3). The contributions of CSA from ^{19}F and ^{13}C nuclei to the R_2 of the coherences present in the ^{13}C-^{19}F TROSY pulse sequence are shown in Supplementary Fig. 4. Any coherence with transverse ^{19}F magnetization ($^{19}F_{x/y}$,$^{19}F_{x/y}{}^{13}C_z$,$^{19}F_{x/y}{}^{13}C_{x/y}$) experiences ~22-fold faster CSA relaxation as compared to that of ^{13}C ($^{13}C_{x/y}$,$^{19}F_z{}^{13}C_{x/y}$), suggesting that it would be beneficial to minimize the time ^{19}F spends in the transverse plane. We estimated that, for a 42 kDa protein, ~30% of the initial magnetization is lost during the first INEPT transfer from ^{19}F to ^{13}C due to relaxation. Consequently, we shortened the pulse sequence by employing an out-and-stay design in which the experiment starts with excitation and indirect encoding of one of the nuclei, ^{13}C or ^{19}F, and ends with the direct detection and encoding of the other. Using this approach, we designed two additional experiments a ^{13}C-^{19}F TROSY, which begins with ^{13}C magnetization and ends on ^{19}F, and a ^{19}F-^{13}C TROSY, which starts with ^{19}F magnetization and ends on ^{13}C, the more slowly relaxing nucleus (Supplementary Fig. 5). These experiments utilize the ST2PT block where the phases of the first 90° pulse in ^{13}C and ^{19}F, respectively, are chosen to observe the upfield $^{13}C_F$ TROSY component (Supplementary Fig. 6).

Although the ^{13}C -^{19}F TROSY was more sensitive than the ^{19}F-^{13}C TROSY, the latter had much better resolution (Fig. 3a-c). Fifteen intense and isolated ^{19}F-^{13}C pairs were detected by the out-and-stay experiments, which correspond to the fifteen Tyr residues in MBP. This resolution

demonstrates the advantage of the 2D experiments, as both the ^{19}F and ^{13}C 1D-spectra of MBP cannot resolve individual resonances (Fig. 3d and 3e).

The ^{13}C- and ^{19}F-detected out-and-stay designs had substantially greater sensitivity than the ^{19}F-detected out-and-back style method. In the ^{19}F-^{13}C TROSY pulse program, we take advantage of the large polarization of ^{19}F with its initial magnetization and the faster longitudinal relaxation of $^{19}F_C$ (T_1 ~0.5s) to allow faster recycling delays than are possible in a design where we start with $^{13}C_F$ magnetization (T_1 ~1.4s) (Supplementary Fig. 7). Furthermore, by starting on ^{19}F, the nuclei with the narrower $^{13}C_F$ TROSY resonances are encoded in the direct dimension, which allows access to high-resolution without sacrificing experimental time.

The choice between the ^{19}F and ^{13}C detected out-and-stay experiments is dependent on the sample concentration, the rotational correlation time of the sample, the sample-dependent spectral width in the individual dimensions, the field strength and the probe design. Although we recorded both ^{19}F- and ^{13}C-detected experiments for comparison and have outlined the advantages of each above, we favour the ^{19}F-^{13}C TROSY pulse program. In this design, the maximum evolution in the indirect ^{19}F dimension is limited to ~20 ms for sensitivity, and the more slowly relaxing ^{13}C is encoded in the direct dimension for >200 ms, giving access to the high resolution unlocked by the ^{19}F-^{13}C TROSY effect.

Comparison of ^{19}F-^{13}C TROSY with ^{1}H-^{13}C TROSY

The TROSY resonances of $^{13}C_F$ in 3-^{19}F Tyr are ~7 times narrower than the corresponding $^{13}C_H$ for systems across a wide range of molecular weights (Supplementary Fig. 8). As an illustration, the linewidth of the $^{13}C_F$ TROSY resonance of a protein with τ_c = 95 ns is narrower than the $^{13}C_H$ TROSY resonance of a protein with τ_c = 15 ns. This is due to the more efficient cross-correlation

process (or TROSY effect) in the ^{19}F-^{13}C system, where the magnitude of the CSA term in the spin Hamiltonian is comparable to the dipole-dipole interaction. Thus, selecting the TROSY component of $^{13}C_F$ will yield sharper lines than those of $^{13}C_H$. To experimentally validate this, we took advantage of the presence of two ^{13}C-labelled carbons in 3-$^{19}F_{13C}$ Tyr. While the carbon at position 3 is bonded to a ^{19}F atom, the carbon at position 5 is bonded to ^{1}H. This labelling pattern allows the measurement of ^{1}H-^{13}C and ^{19}F-^{13}C aromatic TROSY on the same sample. We recorded ^{13}C-detected ^{19}F-^{13}C and ^{1}H-^{13}C TROSY spectra of 3-$^{19}F_{13C}$ Tyr-labelled MBP at 25 °C and at 10 °C (Fig. 4). A 42 kDa MBP at 10 °C, behaves with the relaxation properties of a ~65 kDa protein at 25 °C. At 25 °C, in the ^{19}F-^{13}C TROSY we observe 15 sharp and well-resolved cross-peaks as expected for the 15 Tyr. By comparison, only 12 strong and 2 weaker peaks are observed in the ^{1}H-^{13}C TROSY, and the cross-peaks are clearly broader when compared to their ^{19}F-^{13}C TROSY counterparts. At 10 °C, the advantage of the ^{19}F-^{13}C TROSY compared to the ^{1}H-^{13}C TROSY is more pronounced. ^{19}F-^{13}C TROSY lines are moderately broadened at 10 °C, while the linewidths of the ^{1}H-^{13}C TROSY cross-peaks are severely broadened, so that only two cross-peaks can still be recognized.

The effect of molecular weight on the relaxation of the ^{19}F-^{13}C TROSY component can be further highlighted by comparing the TROSY and the anti-TROSY resonances. (Supplementary Fig. 9). A larger molecular weight system can be mimicked by observation at lower temperatures. The linewidth and intensity of the TROSY resonances were barely affected by lowering the temperature from 25 °C to 10 °C, whereas the anti-TROSY resonances were severely broadened and diminished in intensity.

In addition to the fifteen intense peaks observed for MBP, there are some additional weaker signals observed in the ^{19}F-^{13}C TROSY spectrum (Supplementary Fig. 10). Rotation along the Cγ

-Cβ bond is commonly referred to as an aromatic ring flip and has been previously observed for several aromatic amino acids (non-fluorinated). Some of these ring flips have been shown to be in slow exchange on the chemical shift time scale[23]. In unlabelled Tyr residues this leads to two distinct signals of equal intensity due to the symmetry of the aromatic ring. In contrast, 3-$^{19}F_{13C}$ Tyr is no longer symmetric and the differences between ^{19}F and ^{1}H, e.g. the ability of fluorine to hydrogen bond, could shift the equilibrium towards one conformation, producing the observed additional peaks of lesser intensity

To show the applicability of the ^{19}F-^{13}C TROSY to a more challenging and biologically relevant system, we prepared the 3-$^{19}F_{13C}$ labelled 180-kDa α7 single-ring of the 20S proteasome core particle (CP) from *Thermoplasma acidophilum*[3]. This particle lacks residues 97-103 (including one Tyr), to prevent formation of the α7-α7 subunit[19], and thus, our final construct contained 10 Tyr residues. ^{19}F-^{13}C TROSY spectra at 45 °C (τc = 66 ns), 50 °C (τc = 60 ns)[3, 24] and 60 °C (τc = 50 ns), show 8-10 discrete 3-$^{19}F_{13C}$ Tyr signals (Figure 5).

^{19}F-^{13}C TROSY effect in ribonucleic acids

The aromatic ^{1}H-^{13}C TROSY effect has been previously harnessed to obtain narrow lines in nucleic acid NMR[25], and independently, ^{19}F-substituted nucleobases have been used in the study of nucleic acids, including *in cell* NMR applications[13, 26]. Therefore, we posited that the aromatic ^{19}F-^{13}C TROSY described here could also be applied to nucleic acids. We calculated R_2 to determine the TROSY effect for guanine, uracil, thymine, cytosine and adenine nucleobases, with ^{19}F substitutions in eight different positions (Supplementary Fig. 11). For the following discussion, we will consider a fluorinated nucleotide and its non-fluorinated counterpart, to be part of a nucleic acid with a τ_c of 25 ns measured at 600 MHz.

For a nucleobase harbouring a ^{19}F-^{13}C pair, our calculations predicted that the TROSY component of $^{13}C_F$ would, on average, relax 4 times slower than the equivalent decoupled resonance. Similar to the aromatic amino acids, the cross-correlation of ^{13}C-^{19}F pairs is more effective than that of ^{13}C-^{1}H pairs in nucleic acids (e.g. 5-^{19}F Uracil, Supplementary Fig. 12). This makes the R_2 of the TROSY component on average 3 times slower for $^{13}C_F$ than that of $^{13}C_H$ at the same position. 2-fluoroadenine represents a special case, where the TROSY component of $^{13}C_F$ relaxes 58 times slower as compared to the decoupled resonance, yielding theoretically predicted linewidths of < 1Hz. This $^{13}C_F$ TROSY relaxation rate is approximately 29 times slower than the TROSY component of the corresponding $^{13}C_H$. Intriguingly, the $^{19}F_C$ R_2 rates of several nucleotide configurations are considerably slower than those of aromatic amino acids. For example, the $^{19}F_C$ relaxation rate of the TROSY component in 5-fluorocytosine is only 181 Hz in comparison to the 520 Hz of 3-^{19}F Tyr.

To experimentally observe the ^{13}C-^{19}F TROSY effect in nucleic acids, we synthesized a double stranded 16-mer 5-fluorouracil-substituted DNA. We used natural abundance ^{13}C to record ^{19}F-^{13}C correlations at 5 °C (Fig. 6). An approximate rotational correlation time of 11.6 ns was calculated using HYDRONMR[27]. The coupled ^{19}F-^{13}C HSQC spectrum shows four resonances with a sharp and intense top right component. Similar to what was previously observed for 3-$^{19}F_{13C}$ Tyr, the upfield shifted carbon components are clearly narrower than the downfield counterparts. Figure 6b and c, show selection for the TROSY and anti-TROSY components in the 5-fluoruracil 16-mer at 5 °C, respectively. The TROSY effect can also be observed for the upfield $^{19}F_C$ component, confirming the prediction of an effective $^{19}F_C$ TROSY for 5-fluorouracil.

Discussion:

Fluorinated amino acids and nucleobases are easily incorporated into proteins and nucleic acids, respectively, as demonstrated here and reviewed elsewhere[28, 29]. Indeed, ^{19}F is often considered an isostere of ^{1}H, due to their similar van der Waals radii[30]. Unlike other chemical modifications, fluorine incorporation into the aromatic rings of amino acids seems to have minimal effect on the structure and function of the resulting protein[31], although this might be protein-specific. If incorporation of a given ^{19}F-labelled amino acid is found to be detrimental, fractional labelling can be used to dial down the percentage of incorporation. This strategy was recently applied to improve the stability and spectral quality of 3-fluoro-phenylalanine labelled calmodulin[32].

In general, incorporation of fluorinated aromatic amino acids is usually not a technical obstacle for those proteins that express in high yields in *E. coli*. In our hands, expression of MBP and GB1 yielded 100 mg of purified protein per litre of *E. coli* culture. Other fluorinated aromatic amino acids have been expressed with similarly excellent yields, using auxotrophic strains or by incorporation of 5-fluoroindole as a precursor for 5-fluorotryptophan[33, 34]. However, incorporation of fluorinated aromatic amino acids using yeast or other eukaryotic expression systems will require further optimization. For example, *P. pastoris* strain X33 Δaro1 has been previously used in this context[35], although in this strain incorporation of the fluorinated amino acids was stochastic, yielding mixtures of differentially fluorinated proteins[36]. Additionally, while fluorinated amino acids can be recognized as substrates by aminoacyl-tRNA synthetases (AARSs), their efficiency of recognition is generally worse than that of their natural counterparts. In light of this, efficient incorporation of ^{19}F-labeled aromatic amino acids in a eukaryotic expression system may require directed evolution of AARSs, or co-expression of

AARSs specific for the given non-canonical amino acid. Thus, some additional development of eukaryotic overexpression systems will be needed to further broaden the range of proteins that can be subjected to ^{19}F-^{13}C TROSY.

Site specific ^{19}F resonance assignment can be accomplished through the use of site-directed mutagenesis of the relevant residue or nearby residues[31], in conjunction with an HCCF-COSY experiment[21], or with heteronuclear NOESY (HOESY) between ^{19}F and ^{1}H[37]. Alternatively, one can exploit the scalar coupling between the fluorine nucleus and adjacent aromatic protons[38], or use solvent-induced isotope shift experiments to evaluate solvent accessibility[23, 39]. The latter would greatly benefit from the ^{19}F-^{13}C TROSY effect. The pulse programs described here can be incorporated into the aforementioned NMR experiments, and introduce an additional dimension using the ^{13}C-^{19}F correlation, thus facilitating resonance assignment. The unique chemical shift of the fluorinated ^{13}C resonances at ~150 ppm, separated from the aromatic $^{13}C_H$ resonances (at ~120 ppm), will further aid the assignment of ^{19}F resonances. With the appropriate NMR probe design, experiments that encode both ^{1}H-^{13}C and ^{19}F-^{13}C correlations can be recorded using parallel receivers[40].

The specific NMR probe design we used here does not allow ^{1}H decoupling during the detection period, resulting in lines broadened by not only $^{2}J_{CC}$ couplings (~7 Hz) but $^{2}J_{CH}$ and $^{3}J_{CH}$ couplings as well, as seen in the ^{19}F-^{13}C TROSY spectra of MBP (Fig. 4). Thus, a probe design that allows ^{1}H decoupling during the detection period would result in further improvement of linewidths and signal height. We demonstrate the effect of additional ^{1}H decoupling using a room temperature probe that allows pulsing on ^{1}H, in addition to pulses applied on the ^{13}C and ^{19}F channels (Supplementary Fig. 13). Since the interference of ^{19}F-^{13}C

dipole-dipole coupling and CSA is most effective on $^{13}C_F$ nuclei, and only marginally affects $^{19}F_C$ relaxation rates, the ^{13}C spin could be decoupled during ^{19}F evolution in a ^{13}C-^{19}F TROSY experiment to enhance sensitivity, as done in aromatic ^{13}C-^{1}H TROSY experiments.

The fact that we were able to observe the ~7Hz splitting of the $^{13}C_F$ TROSY resonance (Fig. 2) is a powerful illustration of the linewidth improvements that can be obtained using ^{19}F-^{13}C TROSY. However, the $^{2}J_{CC}$ coupling does introduce additional level of complexity and could be removed by selective ^{13}C labelling or band selective ^{13}C decoupling in a ^{13}C-^{19}F TROSY experiment. Furthermore, it should be noted that 4-^{19}F-^{13}C Phe can be synthesized from commercially available 4-^{13}C Tyr[41]. This amino acid would have a single ^{13}C connected to ^{19}F, thereby obviating the need for ^{13}C decoupling. Fluorinated analogues of tryptophan, 4-, 5-, 6- and 7-fluorotryptophan have been used quite extensively as fluorescent and NMR probes[42, 43]. However, synthesizing the corresponding isotopomers containing a ^{13}C-^{19}F bond is challenging because the ^{13}C-fluoroindole moiety has to be chemically or enzymatically assembled from simpler ^{13}C-labeled precursors[44]. Treatment of tryptophan with an electrophilic fluorinating agent under the conditions reported here for tyrosine yields 3-fluorooxindole instead of fluorotryptophan[45].

The ability to disperse the $^{19}F_C$ peaks with the narrow $^{13}C_F$ resonances provides a new strategy for investigating dynamic processes, including weak binding, enzyme kinetics, conformational exchange, and protein folding, as well as the physical and thermodynamic properties of proteins and nucleic acids[29]. ^{19}F-^{13}C TROSY combined with ^{19}F relaxation dispersion measurements would enable us to monitor a wide range of dynamics at different timescales. The large chemical shift dispersion and the sensitivity of the ^{19}F chemical shift, coupled with the dispersion of the ^{19}F chemical shift by the narrow ^{13}C resonances, enables the

resolution of minor states and the detection of exchange processes (in the range of 100-500 µs) that cannot be explored with traditional ^{13}C- or ^{15}N-relaxation-dispersion experiments[46, 47].

Reduced spectral crowding and the strong $^{1}J_{CF}$ coupling make the ^{13}C-^{19}F spin-pair an excellent tool to measure residual dipolar couplings (RDCs). RDCs provide distance independent information about structure and dynamics[48]. Since the TROSY effect is largely experienced by the ^{13}C nuclei, measuring both resonances corresponding to the $^{13}C_F$ TROSY component, will yield sharp and intense peaks, which could be used to extract residual dipolar couplings (RDC).

The 2D ^{19}F-^{13}C correlation spectrum can also be used in conjunction with protein-observed ^{19}F-fragment screening[28] to elucidate information about the binding sites of fragments on the surface of the protein. The method could further be extended to study the interactions of fluorine-bearing small molecules with bio-molecules, particularly if the cross correlation between the ^{19}F-^{13}C DD and CSA relaxation is favourable.

Fluorinated nucleotides are frequently employed as cancer drug antimetabolites. For example, 5-fluorouracil and its prodrug capecitabine are used for the treatment of cancers, including colorectal, breast, and head and neck malignancies[49]. Fludarabine, a prodrug of 2-fluoroadenosine, has been approved for clinical use for the treatment of leukaemia and has shown strong potential for prostate cancer[50]. However, the mechanisms of action for these drugs are incompletely understood, and their use is associated with serious side effects[50]. With the ^{19}F-^{13}C -TROSY, we could leverage the slow $^{13}C_F$ relaxation predicted for 2-fluoroadenosine and 5-fluorouracil, in combination with *in cell* NMR, to investigate binding, number of targets and metabolism of these drugs.

In summary, we have demonstrated that the ^{19}F-^{13}C TROSY experiment with ^{13}C direct detection can generate spectra with sensitive, high-resolution signals from a high molecular weight system up to 180 kDa. Theoretical calculations of transverse relaxation rates for the $^{13}C_F$, $^{13}C_H$ and the ^{15}N-^{1}H ($^{15}N_H$) TROSY components reveal that the narrow $^{13}C_F$ TROSY resonances are sharper than any other resonance in biological NMR, including the extremely narrow $^{15}N_H$ TROSY resonances (Supplementary Fig. 14). It should also be noted that detection of $^{13}C_F$ TROSY does not need deuteration, which is required for the methyl TROSY. In addition, observing one resonance per aromatic amino acid of choice vastly reduces the spectral complexity as compared to detecting resonances of methyl bearing amino acids.

Given that aromatic residues are critical in providing the structural framework and play an important role in the function of biomolecules, the ^{19}F-^{13}C TROSY we describe here will expand the utility of the existing arsenal of NMR methods and allow the detection of these residues in both high molecular weight systems as well as in biomolecular systems with complex conformational behaviours where standard NMR strategies are impeded.

Acknowledgments: We thank Dr. Kendra E. Leigh and Dr. Milka Kostic for help in proofreading of the manuscript presented here and the discussions regarding the work, and Dr. Donna Baldisseri for her help with the NMR experiments. We are especially grateful to Dr. Lewis E. Kay (Departments of Molecular Genetics, Biochemistry and Chemistry, University of Toronto, Toronto, Ontario, Canada) for sharing the plasmid carrying the single-ring α7 proteasome particle with us. This research was supported by NIH grants GM047467 and AI03758 to G.W. H.A. acknowledges funding from the Claudia Adams Barr Program for Innovative Cancer Research. A.B. thanks the Austrian Science Fund FWF for the Schrödinger

Fellowship J3872-B21. S.C. acknowledges National Health and Medical Research Council Australia for the C. J. Martin Fellowship APP1090444. Maintenance of the NMR instruments used for this research was supported by NIH grant EB002026.

Author contributions:

A.B., S.C., G.W., V.M.G, I.K., K.T., and H.A. designed research; A.B., S.C., A.D., D.L.R, N.T.B., C.D.C., O.I.P., V.M.G., C.A., M.Z., H.K., I.K., K.T., and H.A. performed experiments; A.B., S.C., A.D., V.M.G., H.K., I.K. and H.A. analysed data., and A.B., S.C., A.D., G.W., I.K., D.L.R., V.M.G., K.T., and H.A., wrote the paper.

Competing Financial Interests

The author Vladimir Gelev is the founder of FB Reagents Ltd., a company that provides isotopically enriched NMR reagents and declares a competing interest. Clemens Anklin and Helena Kovacs work for Bruker Biospin Corporation, which is manufacturer of the equipment used in this work.

All other authors declare no competing financial interests.

Correspondence and requests for materials should be addressed to H.A. (hari@hms.harvard.edu) or K.T.(koh-takeuchi@aist.go.jp).

References:

1. Pervushin, K., Riek, R., Wider, G. & Wuthrich, K. Attenuated T2 relaxation by mutual cancellation of dipole-dipole coupling and chemical shift anisotropy indicates an avenue to NMR structures of very large biological macromolecules in solution. *Proc Natl Acad Sci U S A* **94**, 12366-12371 (1997).
2. Pervushin, K., Riek, R., Wider, G. & Wuthrich, K. Transverse relaxation-optimized spectroscopy (TROSY) for NMR studies of aromatic spin systems in 13C-labeled proteins. *J Am Chem Soc* **120**, 6394-6400 (1998).
3. Sprangers, R. & Kay, L.E. Quantitative dynamics and binding studies of the 20S proteasome by NMR. *Nature* **445**, 618-622 (2007).
4. Fiaux, J., Bertelsen, E.B., Horwich, A.L. & Wuthrich, K. NMR analysis of a 900K GroEL GroES complex. *Nature* **418**, 207-211 (2002).
5. Meyer, L.H. & Gutowsky, H.S. Electron Distribution in Molecules. II. Proton and Fluorine Magnetic Resonance Shifts in the Halomethanes. *The Journal of Physical Chemistry* **57**, 481-486 (1953).
6. Solomon, I. Relaxation Processes in a System of Two Spins. *Physical Review* **99**, 559-565 (1955).
7. Sykes, B.D. & Hull, W.E. in Methods in Enzymology, Vol. 49 270-295 (Academic Press, 1978).
8. Liu, J.J., Horst, R., Katritch, V., Stevens, R.C. & Wuthrich, K. Biased signaling pathways in beta2-adrenergic receptor characterized by 19F-NMR. *Science* **335**, 1106-1110 (2012).
9. Kim, T.H. et al. The Role of Ligands on the Equilibria Between Functional States of a G Protein-Coupled Receptor. *J Am Chem Soc* **135**, 9465-9474 (2013).
10. Barhate, N.B., Barhate, R.N., Cekan, P., Drobny, G. & Sigurdsson, S.T. A nonafluoro nucleoside as a sensitive 19f NMR probe of nucleic acid conformation. *Org Lett* **10**, 2745-2747 (2008).
11. Kreutz, C., Kahlig, H., Konrat, R. & Micura, R. A general approach for the identification of site-specific RNA binders by 19F NMR spectroscopy: proof of concept. *Angewandte Chemie* **45**, 3450-3453 (2006).
12. Kiviniemi, A. & Virta, P. Characterization of RNA invasion by (19)F NMR spectroscopy. *J Am Chem Soc* **132**, 8560-8562 (2010).
13. Bao, H.L. et al. Characterization of human telomere RNA G-quadruplex structures in vitro and in living cells using 19F NMR spectroscopy. *Nucleic Acids Res* **45**, 5501-5511 (2017).
14. Gerig, J.T. Fluorine NMR of proteins. *Progress in Nuclear Magnetic Resonance Spectroscopy* **26**, 293-370 (1994).
15. Brindle, K., Williams, S.-P. & Boulton, M. 19F NMR detection of a fluorine-labelled enzyme in vivo. *FEBS Letters* **255**, 121-124 (1989).

16. Li, C. et al. Protein 19F NMR in Escherichia coli. *J Am Chem Soc* **132**, 321-327 (2010).

17. Gronenborn, A.M. et al. A novel, highly stable fold of the immunoglobulin binding domain of streptococcal protein G. *Science* **253**, 657-661 (1991).

18. Gardner, K.H., Zhang, X., Gehring, K. & Kay, L.E. Solution NMR Studies of a 42 KDa Escherichia Coli Maltose Binding Protein/β-Cyclodextrin Complex: Chemical Shift Assignments and Analysis. *J Am Chem Soc* **120**, 11738-11748 (1998).

19. Sprangers, R. et al. TROSY-based NMR evidence for a novel class of 20S proteasome inhibitors. *Biochemistry* **47**, 6727-6734 (2008).

20. Hogben, H., Krzystyniak, M., Charnock, G., Hore, P. & Kuprov, I. Spinach–a software library for simulation of spin dynamics in large spin systems. *J Magn Reson* **208**, 179-194 (2011).

21. Kitevski-LeBlanc, J.L., Al-Abdul-Wahid, M.S. & Prosser, R.S. A mutagenesis-free approach to assignment of (19)F NMR resonances in biosynthetically labeled proteins. *J Am Chem Soc* **131**, 2054-2055 (2009).

22. Nietlispach, D. Suppression of anti-TROSY lines in a sensitivity enhanced gradient selection TROSY scheme. *J Biomol NMR* **31**, 161-166 (2005).

23. Khan, F., Kuprov, I., Craggs, T.D., Hore, P.J. & Jackson, S.E. 19F NMR studies of the native and denatured states of green fluorescent protein. *J Am Chem Soc* **128**, 10729-10737 (2006).

24. Religa, T.L., Sprangers, R. & Kay, L.E. Dynamic regulation of archaeal proteasome gate opening as studied by TROSY NMR. *Science* **328**, 98-102 (2010).

25. Riek, R., Pervushin, K., Fernandez, C., Kainosho, M. & Wuthrich, K. [(13)C,(13)C]- and [(13)C,(1)H]-TROSY in a triple resonance experiment for ribose-base and intrabase correlations in nucleic acids. *J Am Chem Soc* **123**, 658-664 (2001).

26. Seela, F. & Xu, K. DNA with stable fluorinated dA and dG substitutes: syntheses, base pairing and 19F-NMR spectra of 7-fluoro-7-deaza-2'-deoxyadenosine and 7-fluoro-7-deaza-2'-deoxyguanosine. *Org Biomol Chem* **6**, 3552-3560 (2008).

27. García de la Torre, J., Huertas, M.L. & Carrasco, B. HYDRONMR: Prediction of NMR Relaxation of Globular Proteins from Atomic-Level Structures and Hydrodynamic Calculations. *Journal of Magnetic Resonance* **147**, 138-146 (2000).

28. Arntson, K.E. & Pomerantz, W.C. Protein-Observed Fluorine NMR: A Bioorthogonal Approach for Small Molecule Discovery. *J Med Chem* **59**, 5158-5171 (2016).

29. Kitevski-LeBlanc, J.L. & Prosser, R.S. Current applications of 19F NMR to studies of protein structure and dynamics. *Progress in Nuclear Magnetic Resonance Spectroscopy* **62**, 1-33 (2012).

30. Marsh, E.N. & Suzuki, Y. Using (19)F NMR to probe biological interactions of proteins and peptides. *ACS Chem Biol* **9**, 1242-1250 (2014).

31. Danielson, M.A. & Falke, J.J. Use of 19F NMR to probe protein structure and conformational changes. *Annu Rev Biophys Biomol Struct* **25**, 163-195 (1996).

32. Kitevski-LeBlanc, J.L., Evanics, F. & Scott Prosser, R. Optimizing (1)(9)F NMR protein spectroscopy by fractional biosynthetic labeling. *J Biomol NMR* **48**, 113-121 (2010).

33. Gee, C.T. et al. Protein-observed (19)F-NMR for fragment screening, affinity quantification and druggability assessment. *Nat Protoc* **11**, 1414-1427 (2016).

34. Wang, M. et al. Fast Magic Angle Spinning (1)(9)F NMR of HIV-1 Capsid Protein Assemblies. *Angewandte Chemie* (2018).

35. Whittaker, M.M. & Whittaker, J.W. Construction and characterization of Pichia pastoris strains for labeling aromatic amino acids in recombinant proteins. *Protein Expr Purif* **41**, 266-274 (2005).

36. Budisa, N., Wenger, W. & Wiltschi, B. Residue-specific global fluorination of Candida antarctica lipase B in Pichia pastoris. *Mol Biosyst* **6**, 1630-1639 (2010).

37. Watts, J.K. et al. Differential stability of 2'F-ANA*RNA and ANA*RNA hybrid duplexes: roles of structure, pseudohydrogen bonding, hydration, ion uptake and flexibility. *Nucleic Acids Res* **38**, 2498-2511 (2010).

38. Kitevski-LeBlanc, J.L., Evanics, F. & Scott Prosser, R. Approaches to the assignment of 19F resonances from 3-fluorophenylalanine labeled calmodulin using solution state NMR. *J Biomol NMR* **47**, 113-123 (2010).

39. Kitevski-LeBlanc, J.L., Evanics, F. & Prosser, R.S. Approaches for the measurement of solvent exposure in proteins by 19F NMR. *J Biomol NMR* **45**, 255-264 (2009).

40. Kovacs, H. & Kupce, E. Parallel NMR spectroscopy with simultaneous detection of (1) H and (19) F nuclei. *Magn Reson Chem* **54**, 544-560 (2016).

41. Tang, P., Furuya, T. & Ritter, T. Silver-catalyzed late-stage fluorination. *J Am Chem Soc* **132**, 12150-12154 (2010).

42. Frieden, C., Hoeltzli, S.D. & Bann, J.G. The preparation of 19F-labeled proteins for NMR studies. *Methods in enzymology* **380**, 400-415 (2004).

43. Salwiczek, M., Nyakatura, E.K., Gerling, U.I., Ye, S. & Koksch, B. Fluorinated amino acids: compatibility with native protein structures and effects on protein-protein interactions. *Chem Soc Rev* **41**, 2135-2171 (2012).

44. Konas, D.W., Seci, D. & Tamimi, S. Synthesis of (L)-4-Fluorotryptophan. *Synthetic Communications* **42**, 144-152 (2012).

45. Takeuchi, Y., Tarui, T. & Shibata, N. A novel and efficient synthesis of 3-fluorooxindoles from indoles mediated by Selectfluor. *Org Lett* **2**, 639-642 (2000).

46. Kim, T.H. et al. The role of dimer asymmetry and protomer dynamics in enzyme catalysis. *Science* **355** (2017).

47. Hoang, J. & Prosser, R.S. Conformational selection and functional dynamics of calmodulin: a (19)F nuclear magnetic resonance study. *Biochemistry* **53**, 5727-5736 (2014).

48. Schwieters, C.D. et al. Solution structure of the 128 kDa enzyme I dimer from Escherichia coli and its 146 kDa complex with HPr using residual dipolar couplings and small- and wide-angle X-ray scattering. *J Am Chem Soc* **132**, 13026-13045 (2010).

49. Depetris, I. et al. Fluoropyrimidine-induced cardiotoxicity. *Crit Rev Oncol Hematol* **124**, 1-10 (2018).

50. Voeks, D. et al. Gene therapy for prostate cancer delivered by ovine adenovirus and mediated by purine nucleoside phosphorylase and fludarabine in mouse models. *Gene Ther* **9**, 759-768 (2002).

Figure legends:

Figure 1: Theoretical transverse relaxation rates (R_2) of ^{13}C, ^{19}F, and ^{1}H resonances as a function of magnetic field strength. (a) R_2 of $^{13}C_F$ in 3-^{19}F Tyr and (b) R_2 of $^{13}C_H$ in Tyr. (c) R_2 of $^{19}F_C$ in 3-^{19}F Tyr and (d) R_2 of $^{1}H_C$ at position 3 in Tyr. Here 3-^{19}F Tyr (panel A inset) and Tyr are part of a 42 kDa protein with a τ_c of 25 ns. Red squares represent the R_2 of the TROSY component and blue triangles represent the R_2 of the decoupled resonances. The points are connected by a dashed line to provide visual clarity.

Figure 2: TROSY effect observed in a coupled 1D ^{13}C spectrum of GB1 at multiple magnetic field strengths. (a) $^{13}C_F$ as compared to (b) $^{13}C_H$. Linewidths at half height are indicated above the TROSY component of the Tyr $^{13}C_F$ or $^{13}C_H$ resonances, respectively. In (a), the ~7 Hz splitting due to $^{2}J_{CC}$ coupling is highlighted in the inset panel. Linewidth at half height is abbreviated as $LW_{1/2}$. Note that there is no $^{2}J_{CC}$ coupling present in $^{13}C_H$ as it is recorded on natural abundance ^{13}C. Due to signal overlap, only one isolated Tyr $^{13}C_H$ resonance is shown in (b). In the 800 and 900 MHz spectra depicted in (a), one down-field doublet was cut off for clarity.

Figure 3: ^{19}F-^{13}C TROSY experiments for the 42 kDa MBP with different excitation and detection schemes. (a) ^{19}F-start, ^{19}F-detected, (b) ^{13}C-start, ^{19}F-detected, and (c) ^{19}F-start, ^{13}C-detected experiments were recorded on a 700 µM 3-$^{19}F_{13C}$ Tyr-labelled MBP sample, at 600 MHz. The axes were transposed in (c) for easier comparison. (d) 1D ^{19}F spectrum of MBP and (e) 1D ^{13}C spectrum of MBP.

Figure 4: The $^{13}C_F$ TROSY resolves all expected cross-peaks for 3-$^{19}F_{13C}$ Tyr-labelled MBP at 10 °C. Comparison of the ^{1}H-^{13}C (left) and ^{19}F-^{13}C (right) TROSYs of the 5-$^{1}H_{13C}$ and 3-$^{19}F_{13C}$ Tyr spin-pairs at 25 °C (spectra in the top panel) and 10 °C (spectra in the bottom panel).

Figure 5: $^{13}C_F$ TROSY resonances of the 180-kDa proteasome α_7 single-ring particle. ^{19}F-^{13}C TROSY spectra of the 180-kDa proteasome α7 single-ring particle recorded at 45 °C (τc = 66 ns, blue), 50 °C (τc = 60 ns, green) and 60 °C (τc = 50 ns, red), respectively.

Figure 6: TROSY selection of the narrowest component in ^{19}F-^{13}C correlation spectra of a 16-mer 5-fluorouracil-substituted DNA, at 5 °C. a) Coupled HSQC. In b) the top right "TROSY" component, and in c) the bottom left "anti-TROSY" component is selected. The spectra were recorded at 600 MHz, b and c are time-equivalent spectra with equivalent contour levels.

Online Methods:

Synthesis of 3,5-$^{13}C_2$-3-fluoro-L-tyrosine (3-F Tyr)

Selectfluor® was purchased from Fluorochem (Hadfield, UK). HPLC-grade acetonitrile and methanol as well as all other reagents were purchased from Labimex Ltd (Sofia, Bulgaria) and used without further purification. 3,5-$^{13}C_2$-L-tyrosine was purchased from Cambridge Isotope Laboratories (Tewksbury, MA). Preparative HPLC was performed on a Waters® 600 Delta system equipped with a Phenomenex® Luna C-18 column (250 x 21 mm, 5μ) and electrospray ionization mass spectrometry (ESI-MS) detection in the positive mode using a Waters® Micromass ZQ 2000. NMR spectra were recorded on a Bruker 500 MHz spectrometer equipped with an AvanceIII console.

The synthesis follows a modified procedure of Kitevski-LeBlanc *et al.*[21] (Supplementary Note II). L-tyrosine (phenol-3,5-$^{13}C_2$, 95-99%) (100 mg, 0.55 mmol) was suspended in 20 mL of acetonitrile:water (4:1) in a screw cap vial and heated to 80˚C for 30 minutes in a polyethylene glycol 400 bath. The vial was removed from the bath briefly, Selectfluor® (N-Fluoro-N'-chloromethyltriethylenediaminebis(tetrafluoro-borate)) (586 mg, 2.4 equivalents) was added, and the vial was returned to the heating bath. The suspension cleared within minutes and stirring was continued for 1h at 80˚C. The course of the reaction was monitored by mass spectrometry. At the end of the 1 h incubation, the ratio of tyrosine to 3-fluorotyrosine and 3,5-difluorotyrosine was 30:60:10. Longer reaction times or excess of fluorinating agent resulted in larger fractions of difluorinated product, which could not be recycled, unlike unreacted tyrosine. The reaction solution was diluted with 20 mL of 0.1 M HCl and the acetonitrile was evaporated fully under reduced pressure. The remaining aqueous solution was filtered through a 0.45 µm PTFE syringe filter and purified in 5 mL volumes by preparative HPLC with ESI-MS detection. Gradient elution over a 15-min period at a flow rate of 13 mL/min with a starting solvent ratio of 1.25:1.25:97.5 (methanol:acetonitrile:0.1% HCOOH) and an ending solvent ratio of 10:10:80 (methanol:acetonitrile:0.1% HCOOH) was used. Retention times of tyrosine, 3-fluorotyrosine and 3,5-difluorotyrosine were 9.4 min, 10.3 min and 11.8 min, respectively. 3-fluorotyrosine-containing fractions were evaporated under reduced pressure to a film, which was then triturated with diethyl ether to yield 40 mg of tan powder (36% from tyrosine). In addition, another 15 mg of unreacted tyrosine was recovered.

^{1}H NMR (500 MHz CD_3OD:D_2O (1:1)) δ 3.10 (dd, J = 14.7, 7.5 Hz, 1H), δ 3.23 (dd, J = 14.7, 5.5 Hz, 1H), δ 4.08 (dd, J = 7.5, 5.5 Hz, 1H), δ 6.97 (d, J = 8.3, 1H), δ 6.98 (dq, J = 161.3, 8.7 Hz, 1H), δ 7.08 (ddd, J= 11.9, 5.6, 1.63 Hz). ^{13}C NMR (126 MHz, CD_3OD:D_2O (1:1)) δ 118.20

(d, J = 7.2 Hz), δ 151.28 (dd, J = 245.3, 7.2 Hz). ^{19}F NMR (471 MHz, CD_3OD:D_2O (1:1)) δ -136.5 (d, J = 245.3 Hz). LRMS calculated for $C_7{}^{13}C_2H_{11}FNO_3^+$ $[M+H]^+$ 202.08, found 202.12.

Expression and purification of 3-F Tyr GB1, MBP and the single-ring *a*7 particle of the 20S proteasome core particle:

BL21 (DE3) *E. coli* were transformed with plasmids encoding the protein G B1 domain (GB1; pET9d), maltose binding protein (MBP; pMALC4X), or the single-ring α7 particle (α7, modified pET[3]). Cultures were grown at 37 °C in a shaker-incubator in M9 minimal medium supplemented with 2 g/L ^{13}C-glucose and 1 g/L $^{15}NH_4Cl$. To achieve uniform incorporation of 3-$^{19}F^{13}C$ tyrosine, cells were first grown to an optical density of 0.5 measured at a wavelength of 600 nm (OD_{600}). Then 1 g/L glyphosate was added, along with 50 mg/L 3-$^{19}F^{13}C$ L-tyrosine, 50 mg/L L-phenylalanine, and 50 mg/L L-tryptophan for GB1 and MBP expression. α7 was expressed with 80% 3-$^{19}F^{13}C$ L-tyrosine labelling. To this end 70 mg/L L-phenylalanine, 70 mg/L L-tryptophan, 5 mg/L L-tyrosine and 30 mg/L 3-$^{19}F^{13}C$ L-tyrosine were added alongside 1 g/L glyphosate. Cultures were grown to an OD_{600} of 0.7-0.8 at which point protein expression was induced with 1 mM isopropyl β-D-1-thiogalactopyranoside (IPTG). The cultures were incubated for an additional 16 h at 28 °C (MBP and GB1) or 30 °C (α7) to allow for protein expression. Cells were pelleted by centrifugation for 20 min at 4 °C at 3,500 x *g*.

GB1-expressing cell pellets were resuspended in 40 mL of GB1 lysis buffer (50 mM Tris-HCl (pH 8.0), 350 mM NaCl, 10 mM imidazole, 5 mM β-mercaptoethanol (β-ME)) per liter of original bacterial culture and lysed by sonication. Cell debris was removed from the crude lysate by centrifugation at 4 °C for 40 min at 33,000 x *g*. GB1 was purified from the resulting supernatant by gravity-flow affinity chromatography using 5 mL (10-mL of a 50% slurry) of Ni-

NTA resin (Qiagen). After washing the resin with 40 mL of 50 mM Tris-HCl (pH 8.0), 350 mM NaCl, 40 mM imidazole, and 5 mM β-ME, the protein was eluted in an identical buffer containing 350 mM imidazole. GB1 was then further purified using size exclusion chromatography (GE Healthcare Life Sciences, Superdex 75 10/300 GL pre-packed size exclusion chromatography column) into NMR buffer (10 mM Na_2HPO_4 (pH 6.5), 50 mM NaCl, 1mM EDTA).

MBP-expressing cell pellets were resuspended in 40 mL MBP lysis buffer (25 mM Tris-HCl (pH 8.0), 150 mM NaCl, 1 mM EDTA) per liter of original bacterial culture, lysed by sonication, and clarified by centrifugation for 40 min at 4 °C at 33,000 x *g*. The lysate was loaded onto 5 mL of amylose resin. After washing the resin with resuspension buffer, MBP was eluted with the addition of 40 mM D(+)-maltose. MBP was further purified using size exclusion chromatography (GE Healthcare Life Sciences, Superdex 75 10/300 GL pre-packed size exclusion chromatography column) into NMR buffer (10 mM HEPES (pH 6.5), 1mM EDTA, 1mM β-cyclodextrin).

α7 cell pellets were disrupted by sonication, and the insoluble fraction was removed by centrifugation for 40 min at 16,000 rpm. The protein was initially purified by gravity-flow affinity chromatography using 5 ml (10-ml of a 50% slurry) of Ni-NTA resin (Qiagen). After washing the resin with 40 ml of 50 mM Tris-HCl (pH 8.0), 350 mM NaCl, 20 mM imidazole, and 5 mM β-ME, the protein was eluted in an identical buffer containing 350 mM imidazole. The elution fraction was dialyzed against a buffer containing 50 mM Tris-HCl (pH 8.0), NaCl (100 mM), and DTT (1 mM), and the His_6-tag was removed using TEV protease. The digested proteasome was further purified using size exclusion chromatography (GE Healthcare Life Sciences "Superdex 200 10/300 GL") and eluted in 20 mM sodium phosphate buffer (pH: 6.6)

with 50 mM NaCl and 0.5 mM EDTA. The α7 single-ring particle was concentrated to 143 μM, which corresponds to a monomer concentration of 1 mM.

Typically, a 1 L expression culture produced approximately 100 mg GB1 or MBP and 50 mg α7.

5-fluorouracil-substituted DNA:

The 16-mer, double-stranded DNA sample containing a single 5-fluorodeoxyuridine nucleotide was made from two individual strands obtained from IDT (Coralville, IA) as polyacrylamide-purified samples. The 5-fluorodeoxyuridine nucleotide is known to form a base pair with an adenosine nucleotide.

The DNA sequences of the individual strands are shown below.

5' – GCT AGG /**5F-dU**/ CA ATA CTC G - 3'

5' - CGA GTA TTG ACC TAG C – 3'

where /5F-dU/ is the 5-fluorodeoxyuridine nucleotide (refer to Supplementary Note III for the structure).

The samples were annealed in TE buffer (5 mM Tris-HCl (pH 8.0), 1 mM EDTA) by heating to 80 °C and cooling to 20 °C with a ramp of 1 °C/ 5 sec. The concentration of the double stranded DNA 16-mer was determined using an extinction coefficient of 265,113 $L \cdot mol^{-1} \cdot cm^{-1}$. The final concentration was 1.5 mM.

NMR spectroscopy

Experiments were performed on 1 mM GB1, 700 μM MBP, 1 mM α7 single-ring proteasome particle, or 1.5 mM 5-fluorouracil-substituted DNA. All NMR spectra were collected in the indicated NMR buffer at 298 K, unless otherwise noted. All the 2D NMR spectra were processed with NMRPipe[51] and analysed with CcpNmr[52]. The 1D spectra were processed with Bruker TopSpin® (version 3.2).

1D ^{13}C spectra on 3-^{19}F^{13}C Tyr GB1 and unlabelled GB1

The 1D ^{13}C spectra of 3-^{19}F^{13}C Tyr GB1 (1 mM) were collected on 400, 500, 600, 800, and 900 MHz (^{1}H frequency) spectrometers. The 400 MHz spectrometer is a Varian spectrometer equipped with an INOVA console and a room temperature probe. The 500, 600, 800, and 900 MHz (^{1}H frequency) spectrometers are Bruker spectrometers, equipped with cryogenically cooled probes. ^{1}H decoupling was applied during the acquisition and recovery time periods. The 1D ^{13}C spectra of unlabelled GB1 (1 mM) were collected on 500, 600, 800, and 900 MHz (^{1}H frequency) Bruker spectrometers, equipped with cryogenically cooled probes. ^{1}H decoupling was not applied on the unlabelled sample to allow for observation of the TROSY component of the natural abundant $^{13}C_H$ resonance at the 3rd position of Tyr.

2D ^{13}C-^{19}F correlation spectra on MBP.

The spectra of MBP were recorded on a 600 MHz (^{1}H frequency) Bruker spectrometer equipped with a 5mm triple resonance inverse CryoProbe (TCI, ^{1}H tunable to ^{19}F) with ^{1}H/^{19}F, ^{13}C, and

^{15}N frequencies. The ^{1}H channel was tuned to ^{19}F. This configuration does not allow for ^{1}H decoupling.

For the ^{19}F-detected out-and-back HSQC, the spectral width in the indirect ^{13}C dimension was set to 5 ppm and the spectral width in the direct ^{19}F dimension was set to 40 ppm in both decoupled and coupled experiments. 256 complex points (real + imaginary) were collected in the indirect ^{13}C dimension (acquisition time = 170 ms) and 4096 complex points were collected in the direct ^{19}F dimension (acquisition time = 180 ms). 200 and 512 scans were collected for the coupled and decoupled HSQC, respectively, with a recycling delay of 1 second. The carrier frequencies were centred at 151.5 and -134 ppm in the ^{13}C and ^{19}F dimensions, respectively.

For the out-and-back style TROSY experiments (including the sensitivity enhanced version) the spectral width in the indirect ^{13}C dimension was set to 5 ppm and the spectral width in the direct dimension was set to 40 ppm. 128 complex points were collected in the indirect ^{13}C dimension (acquisition time = 170 ms) and 4096 complex points were collected in the direct ^{19}F dimension (acquisition time = 180 ms). The carrier frequencies were centred at 151.5 and -134.0 ppm in the ^{13}C and ^{19}F dimensions, respectively. 200 scans were collected with a recycling delay of 1 seconds. The regular ST2PT and the sensitivity enhanced versions of the experiments were recorded in a time-equivalent fashion with the same acquisition parameters.

Two different types of out-and-stay experiments were recorded with the following parameters:

1) ^{19}F-detected, ^{13}C-^{19}F out-and-stay TROSY: Here the spectral width in the indirect ^{13}C dimension was set to 20 ppm and the spectral width in the direct dimension was set to 40 ppm.

128 complex points were collected in the indirect ^{13}C dimension (acquisition time = 21 ms) and 4096 complex points were collected in the direct ^{19}F dimension (acquisition time = 90 ms). 80 scans were collected with a recycling delay of 2 seconds. The carrier frequency was centred at 151.5 ppm in the ^{13}C dimension and -135.0 ppm in the ^{19}F dimension.

2) ^{13}C-detected, ^{19}F-^{13}C out-and-stay TROSY: Here the spectral width in the indirect ^{19}F dimension was set to 10.6 ppm and the spectral width in the direct ^{13}C dimension was set to 39 ppm. 116 complex points were collected in the indirect ^{19}F dimension (acquisition time = 10 ms) and 4096 complex points were collected in the direct ^{13}C dimension (acquisition time = 348 ms). 80 scans were collected with a recycling delay of 2 seconds. The carrier frequency was centred at 151.5 ppm in the ^{13}C dimension and -135 ppm in the ^{19}F dimension.

To mimic a higher molecular weight system, we recoded the ^{19}F-^{13}C out-and-stay TROSY experiment on MBP at 10 °C. Here the spectral width in the indirect ^{19}F dimension was set to 6.9 ppm and the spectral width in the direct ^{13}C dimension was set to 39 ppm. 32 complex points were collected in the indirect ^{19}F dimension (acquisition time = 4 ms) and 1024 complex points were collected in the direct ^{13}C dimension (acquisition time = 87 ms). 400 scans were collected with a recycling delay of 1 seconds. The carrier frequency was centred at 151.5 ppm in the ^{13}C dimension and -136.25 ppm in the ^{19}F dimension. Spectra generated at 25 °C were truncated when compared to spectra recorded at 10 °C.

2D ^{13}C-detected-^{1}H-^{13}C TROSY on MBP.

Spectra were recorded on 600 MHz (^{1}H frequency) Bruker spectrometers equipped with 5mm CPTCI and CPPTCI Prodigy Z-GRD Cryoprobes at 25 °C and 10 °C, respectively.

At 25 °C the spectral width in the indirect ^{1}H dimension was set to 2 ppm and the spectral width in the direct ^{13}C dimension was set to 52 ppm. 72 complex points were collected in the indirect ^{1}H dimension (acquisition time = 30 ms) and 2048 complex points were collected in the direct ^{13}C dimension (acquisition time = 131 ms). 160 scans were collected with a recycling delay of 1 second. The carrier frequency was centred at 125 ppm in the ^{13}C dimension and 7 ppm in the ^{1}H dimension.

At 10 °C the spectral width in the indirect ^{1}H dimension was set to 2 ppm and the spectral width in the direct ^{13}C dimension was set to 52 ppm. 128 complex points were collected in the indirect ^{1}H dimension (acquisition time = 53 ms) and 2048 complex points were collected in the direct ^{13}C dimension (acquisition time = 131 ms). 400 scans were collected with a recycling delay of 1 second. The carrier frequency was centred at 125 ppm in the ^{13}C dimension and 7 ppm in the ^{1}H dimension.

2D ^{19}F-^{13}C TROSY on the proteasome single-ring α7 particle.

Spectra were recorded on a 600 MHz (^{1}H frequency) Bruker spectrometer equipped with a 5mm inverse triple resonance CryoProbe (TCI, ^{1}H tunable to ^{19}F) with ^{1}H/^{19}F, ^{13}C and ^{15}N frequencies. The ^{1}H channel was tuned to ^{19}F.

All experiments recorded were ^{13}C-detected, ^{19}F-^{13}C out-and-stay TROSYs. The spectral width in the indirect ^{19}F dimension was set to 8 ppm and the spectral width in the direct ^{13}C dimension was set to 97 ppm. 28 complex points were collected in the indirect ^{19}F dimension (acquisition time = 3 ms) and 2048 complex points were collected in the direct ^{13}C dimension

(acquisition time = 70 ms). 1024 scans were collected with a recycling delay of 1 second. The carrier frequency was centred at 151.5 ppm in the ^{13}C dimension and -136.5 ppm in the ^{19}F dimension. The total experiment time was ~8 hours.

2D ^{13}C-^{19}F correlation spectra on GB1 with ^{1}H decoupling. The GB1 spectra were recorded on a 500 MHz (^{1}H frequency) Bruker spectrometer equipped with an Avance III HD console and 5mm triple resonance observe probe (TXO) tuned to ^{19}F, ^{13}C and ^{1}H frequencies. The spectral width in the indirect ^{13}C dimension was set to 5 ppm and the spectral width in the direct dimension was set to 20 ppm. 150 points were collected in the indirect ^{13}C dimension (acquisition time = 238 ms) and 2048 points were collected in the direct ^{19}F dimension (acquisition time = 218 ms). 48 scans were collected with a recycling delay of 1 second. The carrier frequency was centred at 151.5 ppm in the ^{13}C dimension and -134.0 ppm in the ^{19}F dimension. The carrier frequency in the ^{1}H channel was set to 8.0 ppm. During ^{19}F acquisition in the direct dimension, ^{1}H decoupling was applied using a WALTZ-16 scheme[53].

2D ^{13}C-^{19}F correlation spectra on 5-fluorouracil-substituted DNA.

The spectra of the DNA 16-mer containing a 5-fluorodeoxyuridine nucleotide were recorded on a 600 MHz (^{1}H frequency) Bruker spectrometer equipped with a 5 mm inverse triple resonance CryoProbe (TCI, H tunable to F) with $^{1}H/^{19}F$, ^{13}C and ^{15}N frequencies. The spectra were recorded at 5 °C to mimic a larger molecular weight system. Here we recorded a ^{19}F-detected, out-and-back style, coupled HSQC and a ^{19}F-detected, out-and-stay ^{13}C-^{19}F TROSY spectrum. The spectral width in the indirect ^{13}C dimension was set to 3 ppm and the spectral width in the direct ^{19}F dimension was set to 40 ppm. 55 points were collected in the indirect ^{13}C dimension

(acquisition time = 121 ms) and 1024 points were collected in the direct ^{19}F dimension (acquisition time = 45 ms). 256 scans were collected with a recycling delay of 2 seconds. The carrier frequency was centred at 139.0 ppm in the ^{13}C dimension and -165.5 ppm in the ^{19}F dimension.

Calculating the correlation time of 16-mer DNA

The crystal structure of a 16-mer DNA duplex (pdb id: 420D) was used as a proxy for a 16-mer oligo nucleotide to estimate rotational correlation times for 5-fluorouracil-substituted DNA at 5 °C. All water molecules were stripped from the 16-mer DNA duplex and hydrodynamic calculations were performed with HYDRONMR[27]. The recommended value of 3.2 Å was chosen for the atomic element radius. The parameter NSIG (number of values of the radius of the minibead) was set to 6 and SIGMIN and SIGMAX were defined as 1.0 and 2.0, respectively. The temperature was set to 278.15 K and solvent viscosity was set to 1.5215 mPa·s.

T_1 Measurements on $^{13}C_F$ and $^{19}F_C$

The longitudinal relaxation times (T_1) for $^{13}C_F$ and $^{19}F_C$ were estimated using a 1D inversion recovery NMR experiment. The experiments were recorded using GB1 to observe the isolated $^{19}F_C$ and $^{13}C_F$ resonances. The T_1 for $^{19}F_C$ was measured on a Bruker Avance HD NMR spectrometer operating at 500 MHz (^1H frequency) and equipped with a room temperature probe. 8 experiments were recorded with variable inversion recovery delays of 1, 50, 100, 500, 800, 1000, 1500, and 2000 ms. 32 scans were averaged with a recycle delay of 10 s. The carrier frequency was set to -135 ppm.

The T_1 for $^{13}C_F$ was measured on a Bruker Avance NMR spectrometer operating at 500 MHz (^{1}H frequency) and equipped with a cryogenically cooled probe. 24 experiments were recorded with variable inversion recovery delays of 1, 40, 100, 200, 200, 500, 800, 1000, 1250, 1500, 1750, 2000, 2250, 2500, 2750, 3000, 3250, 3500, 3750, 4000, 4250, 4500, 4750, and 5000 ms. 104 scans were collected with a recycle delay of 10 s. The carrier frequency was set to 150 ppm.

The signal intensity was measured using Bruker TopSpin® (version 3.2). The T_1 value was estimated by fitting an exponential curve described by

$$M = M_0(1 - 2e^{\frac{-t}{T_1}})$$

where M_0 corresponds to the intrinsic intensity of the $^{19}F_C$ and $^{13}C_F$ resonances without relaxation.

Simulation of the free induction decay

We simulated free induction decays (FID) for the TROSY components of aromatic $^{13}C_F$ and $^{13}C_H$ spin-pairs, based on transverse relaxation rates calculated for 3-$^{19}F_{13C}$ Tyr and 3-$^{1}H_{13C}$ Tyr. To compare these to ^{1}H-^{15}N spin pairs, we also calculated the FID for the TROSY component of an average ^{1}H-^{15}N spin pair. The FIDs were simulated using the following expression:

$$I_0 \cos(\Omega t)\, e^{-tR_2}$$

Where I_0 is the initial magnetization, t is the evolution time, R_2 is the relaxation rate and Ω is the chemical shift.

The parameters I_0, and Ω were set to 0.005 and 200 Hz respectively. The signal was evolved for 1 s and sampled at 2048 points, captured by variable t. The time domain signal was Fourier transformed and the real part is displayed. The TROSY component linewidths for a macromolecule with τ_c = 25 ns are 1.9, 2.3, and 13.7 Hz, for $^{13}C_F$, $^{15}N_H$, and $^{13}C_H$, respectively. The TROSY component linewidths for a macromolecule with τ_c = 65 ns are 5.0, 6.1, and 35.7 Hz, for $^{13}C_F$, $^{15}N_H$, and $^{13}C_H$, respectively.

Data availability:

Pulse sequences, parameter sets are available as Supplementary Software and at the lab website.

https://artlab.dana-farber.org/19f_13c_aromatictrosy.html

A life sciences reporting summary is available.

References:

51. Delaglio, F. et al. NMRPipe: a multidimensional spectral processing system based on UNIX pipes. *Journal of biomolecular NMR* **6**, 277-293 (1995).

52. Fogh, R. et al. The CCPN project: an interim report on a data model for the NMR community. *Nat Struct Biol* **9**, 416-418 (2002).

53. Shaka, A.J., Keeler, J., Frenkiel, T. & Freeman, R. An improved sequence for broadband decoupling: WALTZ-16. *Journal of Magnetic Resonance (1969)* **52**, 335-338 (1983).

Type of file: figure
Label: 1
Filename: figure_1.eps

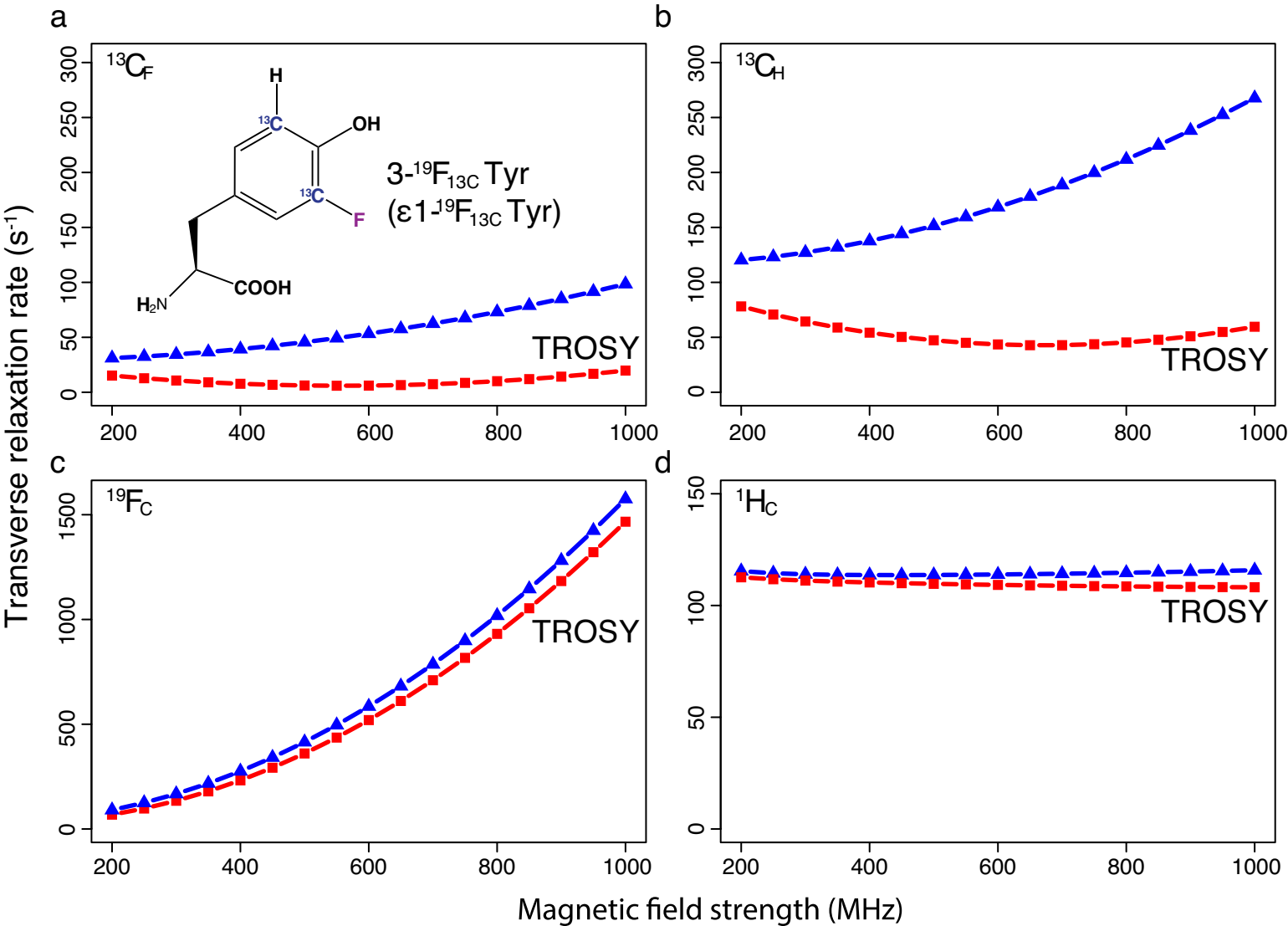
a
b
c
d
$^{13}C_F$
$^{13}C_H$
$^{19}F_C$
^1H_C
3-$^{19}F_{13C}$ Tyr
(ε1-$^{19}F_{13C}$ Tyr)
TROSY
Transverse relaxation rate (s^{-1})
Magnetic field strength (MHz)

Type of file: figure
Label: 2
Filename: figure_2.eps

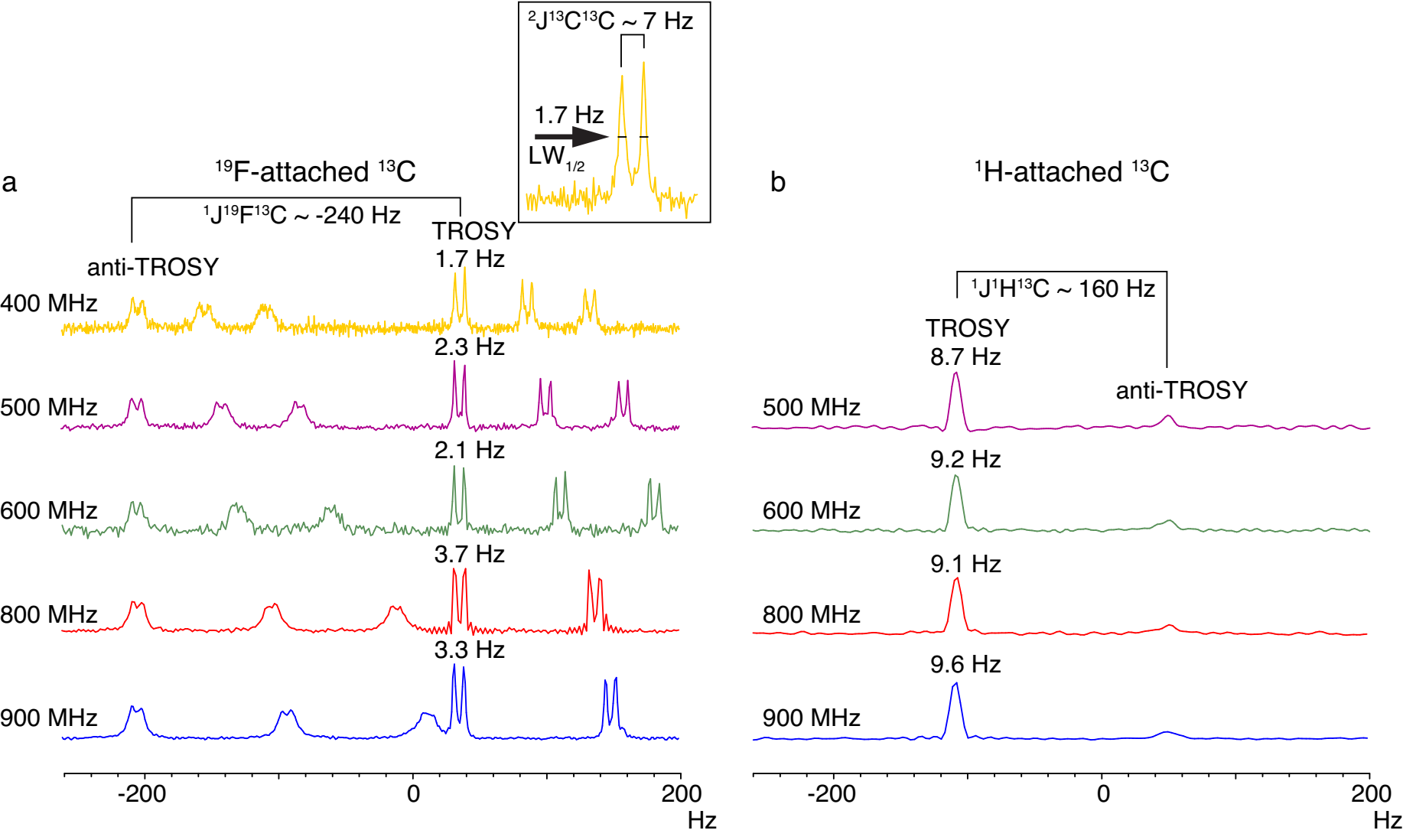
a
^{19}F-attached ^{13}C
$^{1}J^{19}F^{13}C$ ~ -240 Hz
anti-TROSY
TROSY
1.7 Hz
400 MHz
2.3 Hz
500 MHz
2.1 Hz
600 MHz
3.7 Hz
800 MHz
3.3 Hz
900 MHz
-200
0
200
Hz
$^{2}J^{13}C^{13}C$ ~ 7 Hz
1.7 Hz
$LW_{1/2}$
b
^{1}H-attached ^{13}C
$^{1}J^{1}H^{13}C$ ~ 160 Hz
TROSY
8.7 Hz
anti-TROSY
500 MHz
9.2 Hz
600 MHz
9.1 Hz
800 MHz
9.6 Hz
900 MHz
-200
0
200
Hz

Type of file: figure
Label: 3
Filename: figure_3.eps

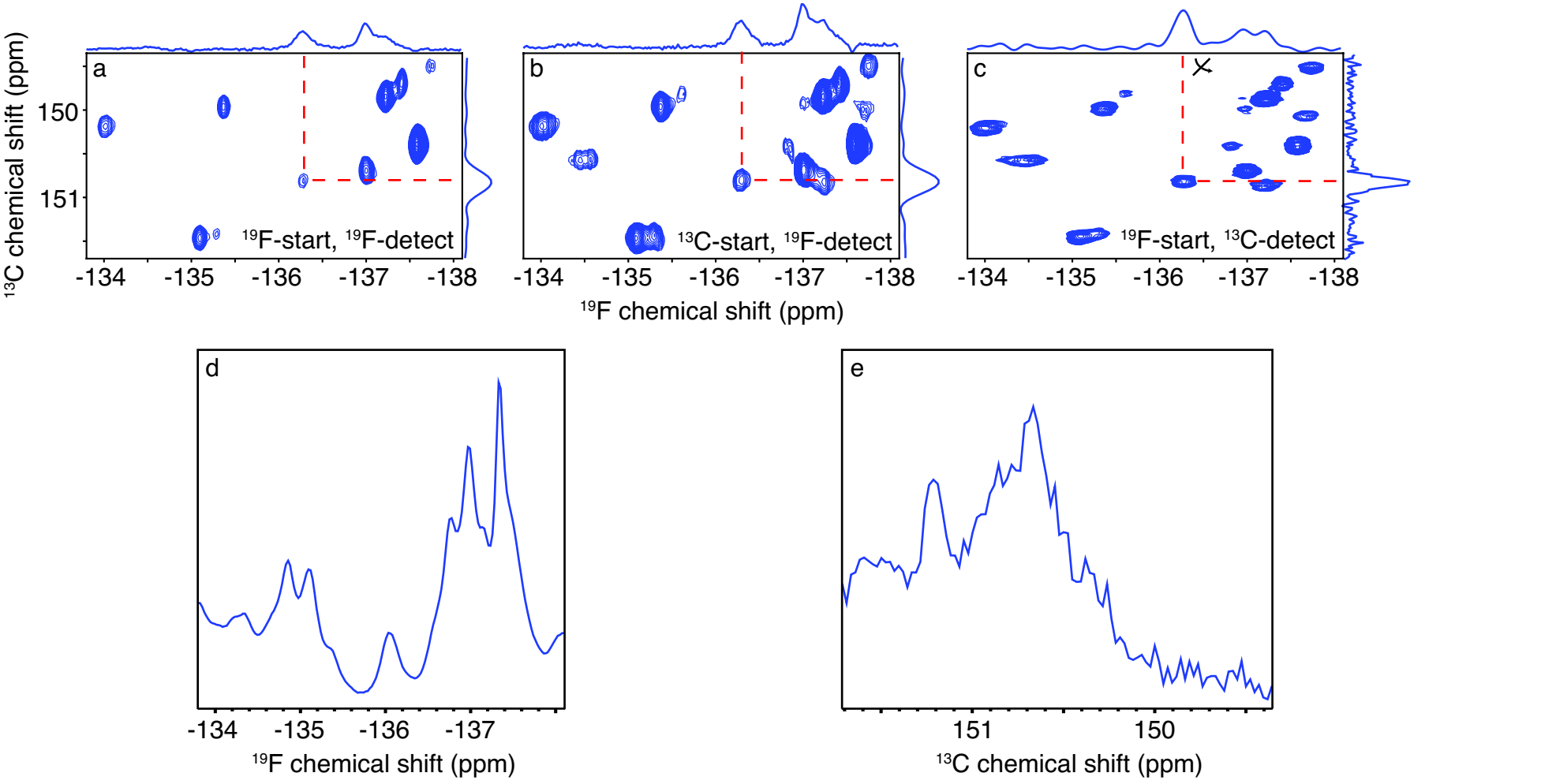
a
b
c
d
e
^{19}F-start, ^{19}F-detect
^{13}C-start, ^{19}F-detect
^{19}F-start, ^{13}C-detect
^{13}C chemical shift (ppm)
150
151
-134
-135
-136
-137
-138
^{19}F chemical shift (ppm)
151
150
^{13}C chemical shift (ppm)

Type of file: figure
Label: 4
Filename: figure_4.eps

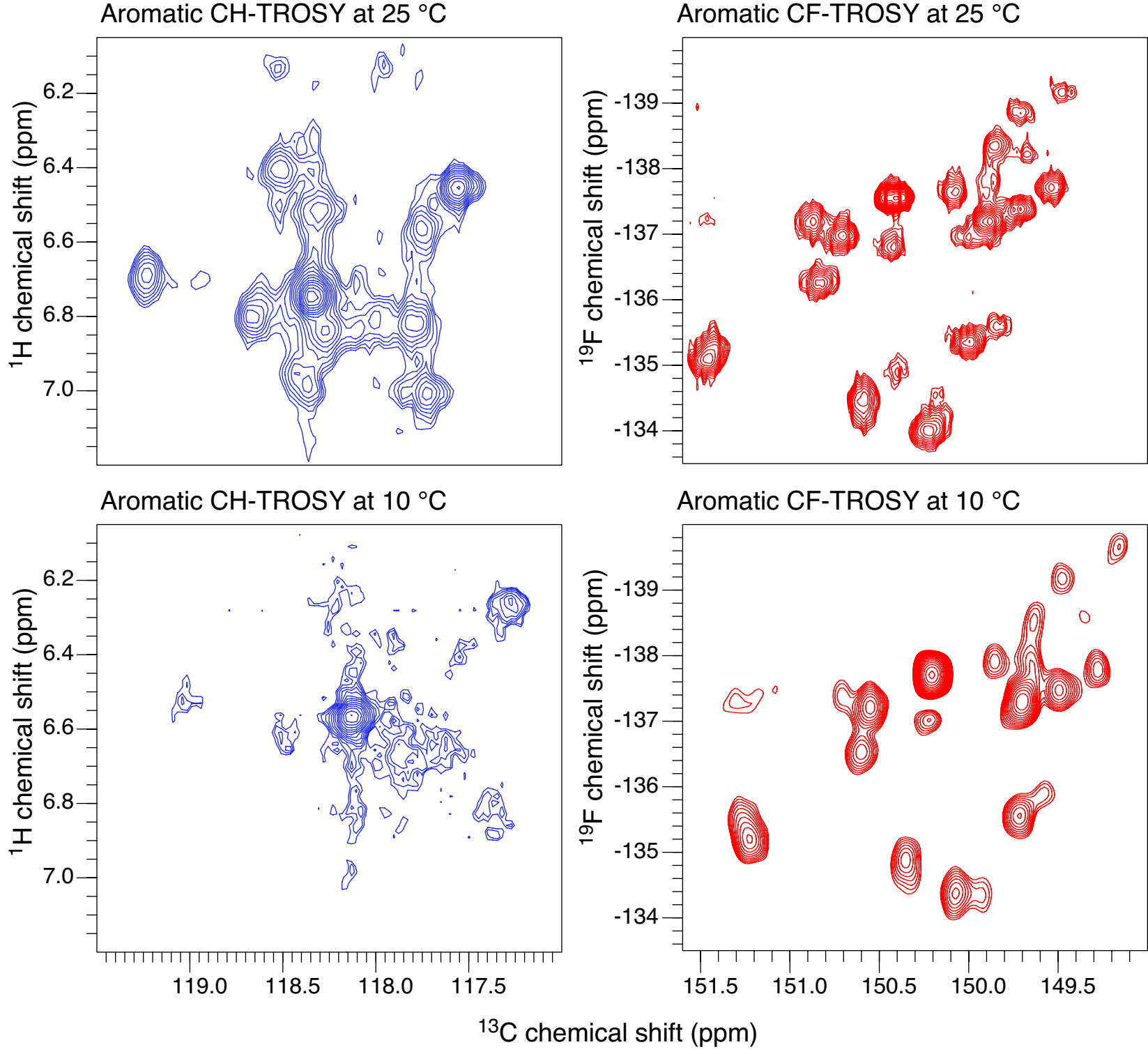
Aromatic CH-TROSY at 25 °C
Aromatic CF-TROSY at 25 °C
Aromatic CH-TROSY at 10 °C
Aromatic CF-TROSY at 10 °C
^{1}H chemical shift (ppm)
^{19}F chemical shift (ppm)
^{13}C chemical shift (ppm)
6.2
6.4
6.6
6.8
7.0
-139
-138
-137
-136
-135
-134
119.0
118.5
118.0
117.5
151.5
151.0
150.5
150.0
149.5

Type of file: figure
Label: 5
Filename: figure_5.eps

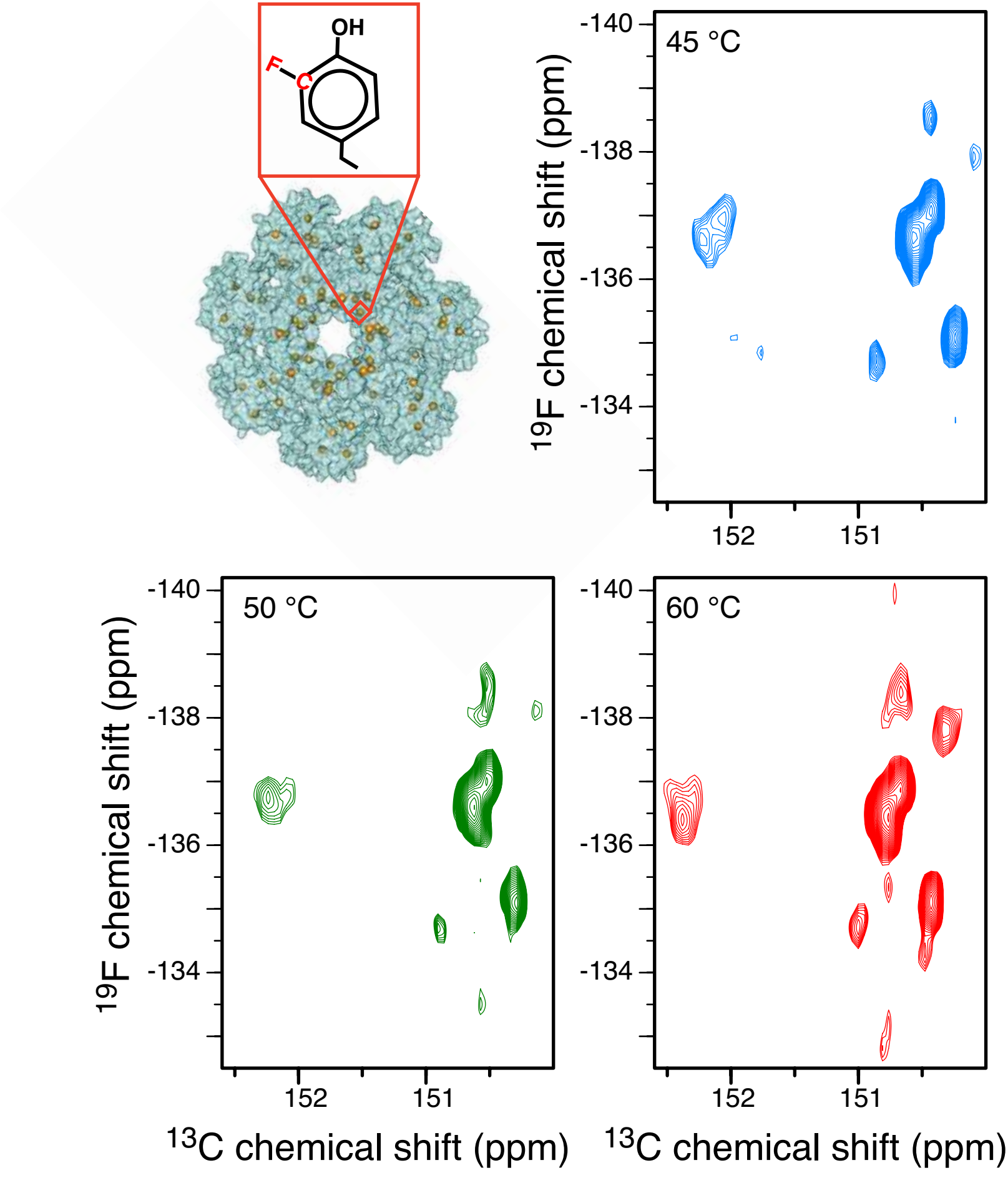
OH
F
C
45 °C
50 °C
60 °C
-140
-138
-136
-134
152
151
^{19}F chemical shift (ppm)
^{13}C chemical shift (ppm)

Type of file: figure
Label: 6
Filename: figure_6.eps

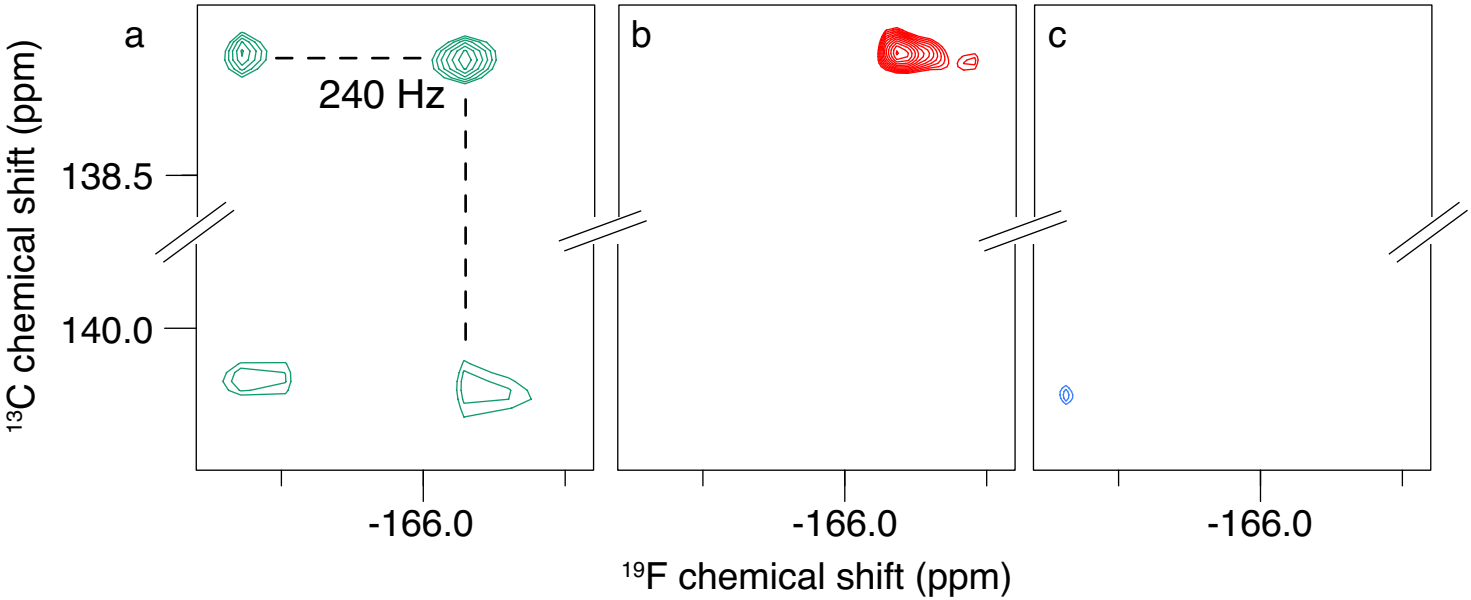
a
b
c
240 Hz
138.5
140.0
-166.0
-166.0
-166.0
^{13}C chemical shift (ppm)
^{19}F chemical shift (ppm)

The NIHMS has received the file 'supp_info_2.pdf' as supplementary data. The file will not appear in this PDF Receipt, but it will be linked to the web version of your manuscript.

The NIHMS has received the file 'supp_info_1.pdf' as supplementary data. The file will not appear in this PDF Receipt, but it will be linked to the web version of your manuscript.

The NIHMS has received the file '43634_3_supp_469173_pjjn86.docx' as supplementary data. The file will not appear in this PDF Receipt, but it will be linked to the web version of your manuscript.

The NIHMS has received the file '43634_3_data_0_pm5lkm.zip' as supplementary data. The file will not appear in this PDF Receipt, but it will be linked to the web version of your manuscript.